Bioinspiration & Biomimetics

PAPER

Flow-induced self-sustained oscillations in a straight channel with rigid walls and elastic supports

RECEIVED
16 March 2022

REVISED
12 July 2022

ACCEPTED FOR PUBLICATION
23 August 2022

PUBLISHED
15 September 2022

Dario Alviso[1,2], Denisse Sciamarella[3], Alejandro Gronskis[1] and Guillermo Artana[1,*]

[1] Laboratorio de Fluidodinámica, Facultad de Ingeniería, Universidad de Buenos Aires, Av. Paseo Colón 850 CABA, Argentina
[2] Universidad María Auxiliadora, Ruta Traschaco Km 12.5, Loma Pyta, Paraguay
[3] Institut Franco-Argentin d'Études sur le Climat et ses Impacts, IFAECI IRL 3351 (CNRS-CONICET-UBA-IRD), Buenos Aires, Argentina
[*] Author to whom any correspondence should be addressed.

E-mail: gartana@fi.uba.ar

Keywords: flow induced self-oscillation, straight channel, fluid-structure interaction

Abstract

This work considers the two-dimensional flow field of an incompressible viscous fluid in a parallel-sided channel. In our study, one of the walls is fixed whereas the other one is elastically mounted, and sustained oscillations are induced by the fluid motion. The flow that forces the wall movement is produced as a consequence that one of the ends of the channel is pressurized, whereas the opposite end is at atmospheric pressure. The study aims at reducing the complexity of models for several physiological systems in which fluid-structure interaction produces large deformation of the wall. We report the experimental results of the observed self-sustained oscillations. These oscillations occur at frequencies close to the natural frequency of the system. The vertical motion is accompanied by a slight trend to rotate the moving mass at intervals when the gap height is quite narrow. We propose a simplified analytical model to explore the conditions under which this motion is possible. The analytical approach considers asymptotic solutions of the Navier–Stokes equation with a perturbation technique. The comparison between the experimental pressure measured at the midlength of the channel and the analytical result issued with a model neglecting viscous effects shows a very good agreement. Also, the rotating trend of the moving wall can be explained in terms of the quadratic dependence of the pressure with the streamwise coordinate that is predicted by this simplified model.

1. Introduction

The cardiovascular or the respiratory system provides abundant examples in which the flow is driven through a deformable channel or tube and where the flow-structure interactions are of major biological importance. In the problem of blood flow, a large part of the attention of researchers has focused on the induced streaming flow and the associated increase of flow rate or changes in solute concentration distribution. Coronary flows [1], working muscles irrigation [2], and oxygen supply to the heart [3] are some paradigmatic examples of this application. This kind of approach is found in the respiratory system of some insects, such as ground beetle [4] and *Lethocerus uhleri* [5], or in the myoelastic-aerodynamic mechanism responsible for voice production in songbirds and mammals [6].

To analyze these complex phenomena in laboratory environments, many authors have considered the Starling resistor. A large number of studies, either experimental or numerical, have been reported [7].

Secomb [1] found that in axisymmetric wall geometries like those of many physiological systems, the flows follow the same lines as in two-dimensional channel flow problems. Hence, studies with this last geometry may provide useful insights into more complex problems. To avoid the problem of flow-induced wall deformation, systems may be further simplified. This naturally leads to the study of flows in channels with moving indentations or with oscillating rigid parallel-sided walls.

The complexity of the modelling of the flow inside these moving-wall channels is mainly due to the moving boundaries of the domain and to the forced wall motion induced by fluid dynamic forces.

Furthermore, the occurrence of the flow detachment from the wall ends may result in oscillatory flows downstream of the moving wall that may interact with the flow inside the channel. A large number of studies with moving indentation have focused their attention on the analysis of the downstream structures when the wall motion is imposed. Stephanoff *et al* [8] studied the fluid flow along a two-dimensional closed channel with an asymmetric oscillating constriction. They observed a train of waves, which appeared in the core flow downstream of the oscillating constriction. Flow along a 2D channel with a moving indentation in one wall was experimentally studied by Pedley and Stephanoff [9]. They considered a steady inflow, and the indentation of the channel moved sinusoidally with time. Downstream the constriction, they found a vortex wave for both viscous and inviscid flow, but there were significant differences between the two cases. A much more complex pattern was obtained in the viscous case, including 'vortex doubling' in which a vortex that initially shows a high degree of longitudinal symmetry becomes markedly asymmetric and eventually splits into at least two separate co-rotating vortices. Ralph and Pedley [10, 11] numerically studied fluid flow through a channel with a moving indentation. Demirdžić and Perić [12] developed a finite volume method for the prediction of fluid flow in arbitrarily shaped domains with moving boundaries. They have validated their method for the flow in a channel with a moving indentation, which has been studied experimentally by Pedley and Stephanoff [9]. Finally, a numerical model used to simulate the flow in a tube with an indentation moving at a given frequency was studied by Ben-Mansour *et al* [13].

Flow-induced oscillations of a parallel-sided channel have been largely discussed, particularly in the context of voice production [14–18]. In these systems, the human vocal folds act as a self-oscillating valve that induces pressure waves upstream and downstream from the glottis in a water-hammer mechanism [19–22]. Mathematical modeling of the flow-induced vocal-fold motion with low-order models usually relies on strong approximations. The geometry of the folds is customarily simplified and the glottal flow is assumed in most cases to be one or quasi-one-dimensional (in space) and quasi-steady (in time) [23]. Idealized vocal-fold models normally consider a symmetric motion of both (left and right) folds, except when trying to model vocal fold unilateral paralysis, in which only one of both folds moves [24].

This kind of problem is not restricted to the physiological domain and can also be encountered in numerous and diverse problems such as lubrication [25–27], peristaltic pumps [28–30], valves [31–34], pulsating diaphragms [35] or in aerodynamic particle focusing devices [36].

When the wall channels are rigid and large enough, the flow can be elegantly described in terms of an exact self-similar solution of the Navier–Stokes equation. This derivation involves an assumption concerning a form of the flow field that enables reducing the equations of motion to an ordinary differential equation for the similarity function [37]. In the present case, the assumption can be posed in terms of the independence of the velocity component (v) in the direction normal to the wall (y) with the longitudinal coordinate (x). Considering incompressibility, the longitudinal velocity (u) has a linear dependence with x. When the boundary conditions at both channel ends are constant and exactly the same, no external pressure gradient is imposed, and the flow exhibits a stagnation point in the symmetry plane at the mid-length of the channel ($x = 0$). This kind of problem belongs to a more general class, that gathers flows in which stagnation points approach oscillatory walls or vice-versa. One of the pioneering works addressing this issue can be found in Rott [38]. Therein, a self-similar solution is found when a plate is set to perform periodic oscillations in the presence of a steady orthogonal flow towards the wall. A large number of similar case studies followed this work, as reviewed in Blyth and Hall [39].

In the particular case of channel flows with oscillating walls, one of the prominent studies was reported in Secomb [1]. This work analyzed both walls moving periodically and symmetrically along the normal direction. The author found asymptotic solutions for u_1: the part of the longitudinal velocity that presents a dependence with x. It depends in fact on the values of two parameters, namely, non-dimensional oscillation amplitude Δ and the Womersley number $\alpha = a_0\sqrt{\frac{\omega}{\nu}}$, with a_0 the half-width of the channel, ω a characteristic frequency, and ν the kinematic viscosity. An interesting aspect of this study was that the author showed that the solution found for u_1 was valid even when an external gradient of pressure was imposed on the channel.

The perturbation technique used in Secomb [1] was also considered by other researchers, who analyzed flows with non-periodic squeeze rates. Some of these studies [40, 41] were performed in terms of the perturbation theory considering the small Reynolds number range. However, several authors highlighted that, even though an initial transient may exist in which such solutions fail, the regular perturbation solution provided accurate results in a larger Reynolds number range, which extended up to $\mathrm{Re} \approx 10$ [42].

Other related problems in which one of the walls remains fixed while the other wall moves vertically were also analyzed by different researchers. These works studied the induced flows for periodic laws of wall motion [43] or transient movement that reduced [27, 44, 45] or increased [46] the clearance between plates.

We found in the vast previous studies involving flows in channels with straight parallel walls and

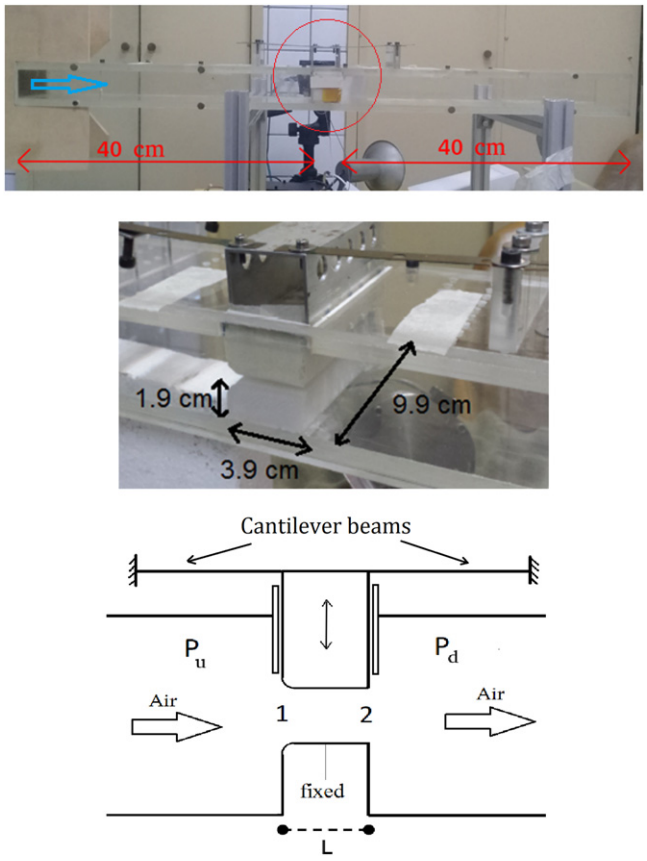

Figure 1. Experimental setup. P_u and P_d are the upstream and downstream pressures, and L is the mass length. The lower mass is maintained fixed while the upper is elastically mounted.

oscillating gap heights, that authors have conventionally considered approaches that do not involve the fluid-structure interaction. This article focuses on the induced motion produced by air flowing inside a channel with rigid parallel walls, one elastically mounted and the other fixed. The purpose of the article is to analyze the dynamics of this system by combining an experimental study and an analytical approach that considers asymptotic solutions of the Navier–Stokes equation with a perturbation technique. An analysis of the channel oscillations is done, considering the frequency spectrum. Our results show that oscillations of the channel wall occur at frequencies close to the natural frequency of the system. Experimentally, a rotating trend of the moving wall is observed, and an explanation of this phenomenon is given. Finally, a comparison between the experimental and analytical pressure at the midlength of the channel is done.

The article is organized as follows: section 2 describes the experimental setup. Section 3 details the model we put forward, considering asymptotic solutions for different cases. In section 4, we discuss the flow-induced vibration of the wall in the context of the analytical models, and section 5 enumerates the most salient aspects of our study.

2. Experimental study

2.1. Setup

The experimental setup shown in figure 1 was chosen to analyze the flow-induced oscillations of a channel. The setup was inspired by a previous one used by Šidlof *et al* [47] to study vocal fold motion.

Inside a rectangular duct of 4 cm × 10 cm, two parallel masses were laid out to throttle the flow in a narrow parallel channel. The leading edges of these masses were rounded to produce a smooth constriction of the flow. A fan produced the airflow along the duct and channel. Labels P_u and P_d denote the upstream and downstream pressure. Typical values of the pressure difference $P_u - P_d$ were close to 150 Pa. Mass dimensions were such that the channel length L along the stream-wise direction x was 3.9 cm and the width in the spanwise direction was 9.9 cm. The gap height $a(t)$ was variable with time and typically followed an approximate sinus law.

The lower mass was fixed while the upper one was linked to two identical cantilever beams on both sides. This support enabled the mass to oscillate vertically as a consequence of the flow. Typical values of the amplitude of oscillations Δ were about 5 mm.

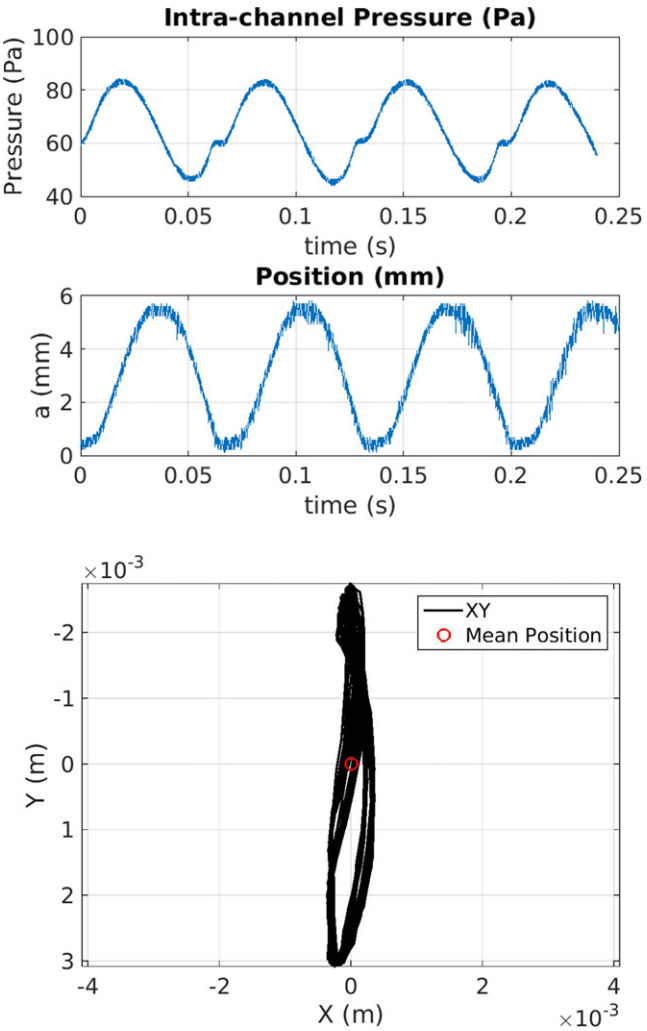

Figure 2. (Left) Pressure evolution in time at the mid-length of the lower mass (top). Gap height against time (below). (Right) Trajectory of the mark point #1 of the upper mass located at 4 mm from the leading edge and from the channel wall.

To minimize the lateral movement produced by the drag exerted on the mass by the flow, two vertical thin plates facing both sides were added to the setup, at the front and the rear part of the oscillating mass. A small airflow settled through the narrow gap between the mass and the plates, producing a lubrification effect that helped compensate for the horizontal movement of the mass. This arrangement also allowed for keeping the upstream pressure at a relatively constant value, when the gap height was largely reduced.

2.2. Mean flow velocity

To characterize the airflow through the channel, its mean velocity was measured at the exit of the duct using a hot wire anemometer (testo 405i Smart). When the masses were oscillating, measurements performed at a frequency of 0.5 Hz showed that far downstream of the channel there was little variation of the flowrate at this frequency, whereas its mean value was ≈6 l/s. In this case, the mean velocity in the channel can be estimated to be circa 1.5 m s^{-1}.

2.3. Pressure difference

The pressure differences at different positions were measured using a variable reluctance low differential pressure manometer (Validyne DP103). The manometer measured the pressure differences using plastic tubes (9 mm diameter and 40 cm length) placed carefully at the positions of interest. The evolution of the upstream pressure 25 cm upstream of the constriction was recorded. The pressure difference was found to remain almost constant in time (around 126 Pa), with fluctuations of the order of 1 Pa. The time dependence of the pressure at the mid-length of the lower mass is shown in figure 2 (left). A cyclic behavior was observed, in which the pressure approximately followed a sinusoidal law. The difference between maximum and minimum pressures was about 35 Pa. Notice that the vertical movement of the mass was synchronized with the pressure signal.

2.4. Upper mass trajectory

The time variation of the channel height was measured using an inductive sensor (Truck type NI8-M18-LIU). This sensor was set to measure the

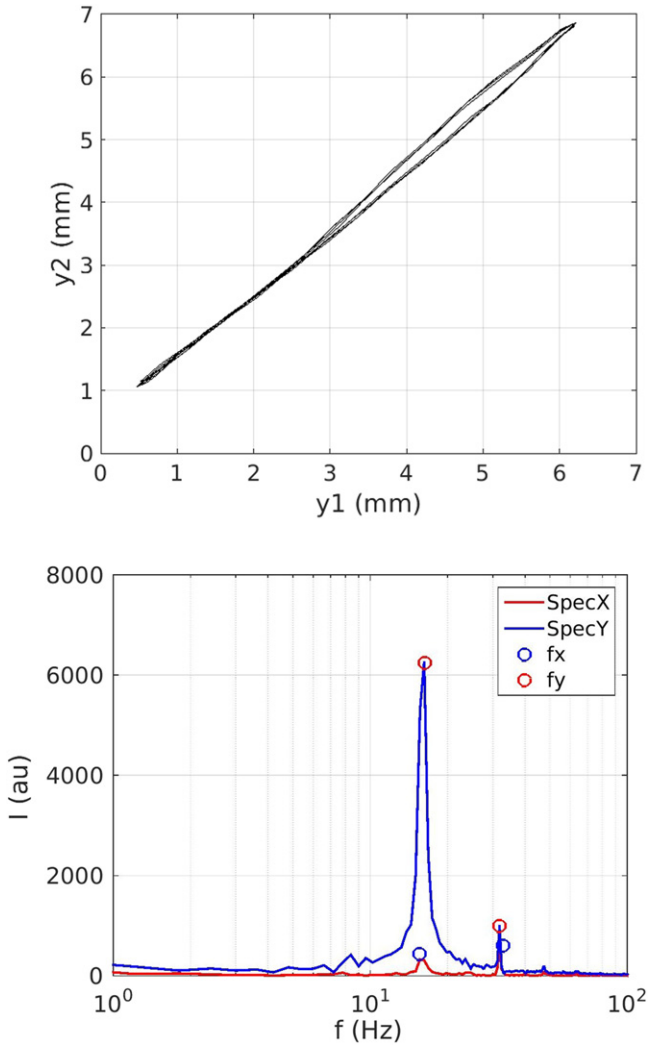

Figure 3. (Left) Vertical movement of mark point #1 and mark point #2, located respectively at 4 mm from the leading and trailing edge in the *x*-direction, and 4 mm from the channel wall in the *y*-direction. (Right) A typical Fast Fourier transform (FFT) of the upper mass movement in the *y*-axis (in blue) and the *x*-axis (in red).

vertical movement of the upper mass. To check that the motion was mainly vertical, mass motion was visualized with image post-processing. The record presented 600 frames per second obtained with a fast camera (512 × 512 pixels SpeedCam MiniVis e2 camera Weinberger) equipped with a 60 mm f/2.8D lens (Micro-Nikkor), located 1 m away from the device. Image resolution was ±70 μm.

The upper mass trajectory was tracked by marking points on it (named 1: left and bottom, and 2: right and bottom of the mass). The vertical motion of the mass was accompanied by a slight rotation that produced a horizontal displacement, as also observed in a similar setup by [47]. A typical trajectory of a mark point is shown in figure 2 (right): the mass moved less than 0.5 mm across the *x*-axis and about 6 mm on the *y*-axis of the mark. In figure 3 (left), points laying off a 1 : 1 slope indicated a slight rotation of the mass (ordinate of point 1 vs ordinate of point 2).

Figure 3 (right) presents the fast Fourier transform (FFT) of the upper mass movement, showing that the frequency of the flow-induced oscillations was close to 15 Hz; harmonics can be observed mainly at 30 Hz.

To estimate the natural frequency (f_n), and the elastic (k) and damping (γ) constants of the system, an impulse test was performed without airflow. The upper mass was released from the highest point. The gap in the rest state was ≈3.9 mm. The upper mass and the cantilever beams (m) were weighed and the value obtained was 124 g.

The damped oscillatory movement of the mass (y_M) was assumed to be described with the following equation [48]:

$$\ddot{y}_M + 2\gamma\dot{y}_M - \omega_0^2 y_M = -g \qquad (1)$$

whose solution is:

$$y_M = A\ \exp(-\gamma t)\sin(\omega t + \varphi) + y_0 \qquad (2)$$

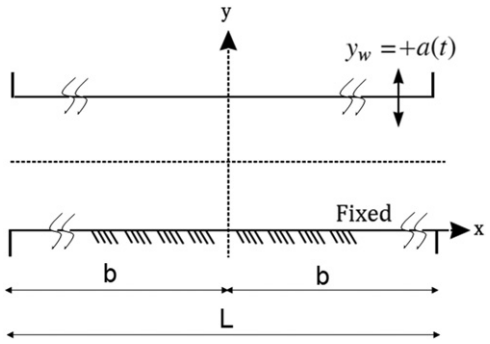

Figure 4. Geometry scheme used for the analytical approach. The length L is much larger than the gap between masses.

where $\omega_0^2 = k/m = 2\pi f_n$, $\omega^2 = \omega_0^2 - \gamma^2$, g is the gravity acceleration, A is the initial amplitude, φ is the initial phase, and y_0 is the gap in the rest state.

A least-square estimation of the parameters of the damped oscillatory equation was performed, yielding:

- $f_n = 14.9$ Hz;
- $k = 1082$ N m^{-1} and
- $\gamma = 19.5$ s^{-1}

3. Problem modelling

Let us now consider a laminar two-dimensional flow of an incompressible fluid in a channel whose half-length ($b = L/2$) is much larger than its mean width (a_o). We assume that the channel ends are connected to large fluid reservoirs, both at constant but different pressure. We can classify this problem as a plane Poiseuille flow with time-varying gap height. A scheme of the geometry is shown in figure 4.

Our interest is laid in those regions where the flow is fully developed and is not affected by the exit/entrance conditions of the fluid. Let us focus on the case in which one of the rigid walls experiences a periodic motion along the normal direction (y-axis) expressed as:

$$y_w = a(t)$$

The equations of motion of this flow are:

$$u_t + uu_x + vu_y = -\phi_x + \nu(u_{xx} + u_{yy}) \tag{3}$$

$$v_t + uv_x + vv_y = -\phi_y + \nu(v_{xx} + v_{yy}) \tag{4}$$

$$u_x + v_y = 0 \tag{5}$$

with (u, v) denoting the velocity components and the ratio between pressure and density $\phi = \frac{p}{\rho}$.

Boundary conditions at $y = y_w$ and $y = 0$ are such that: $u = 0$ and $v = \dot{a}$ and $v = 0$ at the moving and fixed wall respectively. The dot indicates time derivation.

3.1. Self-similar solutions

Let us consider the following transformation of the y-coordinate as $\eta = \frac{y}{a(t)}$, and suppose that the component of the velocity normal to the wall does not depend on the longitudinal coordinate:

$$v(\eta, t) = \dot{a} f(\eta). \tag{6}$$

The incompressible condition then leads to:

$$u = U - \frac{\dot{a}}{a(t)} x f_\eta(\eta) \tag{7}$$

where the subindex indicates derivation with respect to the indicated variable. U does not depend on the x or η coordinate and is associated with the inlet/outlet condition of the channel. Substitution into the Navier–Stokes equation of these expressions and derivation to eliminate pressure gives:

$$f_{\eta\eta\eta\eta} = \frac{a\dot{a}}{\nu}(f_{\eta\eta\eta} f - f_\eta f_{\eta\eta} - \eta f_{\eta\eta\eta} - 2f_{\eta\eta}) + \frac{a^2\ddot{a}}{\nu\dot{a}} f_{\eta\eta} \tag{8}$$

Self-similarity requires satisfying one of these conditions:

Condition 1:

$$\frac{a\dot{a}}{\nu} = C_1 \qquad \frac{a^2\ddot{a}}{\nu\dot{a}} = C_2 \tag{9}$$

Condition 2:

$$f_{\eta\eta\eta\eta} = 0 \tag{10}$$

$$\frac{a\ddot{a}}{\dot{a}^2} = C_0 \tag{11}$$

Condition 3:

$$f_{\eta\eta} = 0 \tag{12}$$

where C_0, C_1, and C_2 are constants. The first condition is satisfied when $a(t)$ scales as $t^{\frac{1}{2}}$. Condition 2 is satisfied if $a(t)$ is sinusoidal. Condition 3 does not impose any restriction on $a(t)$.

3.2. Asymptotic solutions

The set of equations (3)–(5) can be solved numerically with the strategies detailed in [49–51]. These studies are however somewhat arduous as there are transients before the solution is reached, and require special care to attain suitable numerical accuracy. To avoid these difficulties, one possibility is to consider asymptotic solutions. The price to pay is that the solutions may be restricted to a limited range of non-dimensional control parameters.

3.2.1. The non-dimensional equations

Let us now propose the following scaling:

$$\zeta = \frac{x}{b}; \quad t^* = t \times \omega; \quad u^* = \frac{u}{U_0}; v^* = \frac{v}{a_0 \Delta\omega}; \quad \phi^* = \frac{\phi}{U_0^2}$$

where $\phi = \frac{p}{\rho}$ and $\delta = \frac{a_0}{b} \ll 1$. Depending on the case under study, the value of U_0 can be associated with a mean flow velocity produced as a consequence of the gradient of pressure imposed on the channel (i.e.: $U_0 \approx \sqrt{\frac{p_u - p_d}{\rho}}$), or to the longitudinal velocity associated with the squeeze flow produced by the wall movement (i.e.: $U_0 \approx b\omega\Delta$).

For the sake of simplicity, the same notation is kept for the non-dimensional variables as for those previously used, adding an asterisk to indicate that they are in dimensionless form. The height of the channel can be expressed in terms of a general function H and a_0 as:

$$a(t) = a_0 H(\Delta, \omega, t)$$

and the time derivative of the gap height as:

$$\dot{a} = a_0 \omega \dot{H} \Delta$$

Here, ω is the frequency and $\Delta < 1$ determines the amplitude of the oscillation. We only consider cases in which $a > 0$.

This scaling allows rewriting the Navier–Stokes equations in terms of the non-dimensional variables:

$$\left(\frac{b\omega}{U_0}\right) u^*_{t^*} + u^* u^*_\zeta + \left(\frac{b\omega\Delta}{U_0}\right)(\upsilon^* - \dot{H}\eta)\frac{u^*_\eta}{H} = -\phi^*_\zeta + \left(\frac{\nu b}{U_0 a_0^2}\right)\left(u^*_{\zeta\zeta}\delta^2 + \frac{u^*_{\eta\eta}}{H^2}\right) \quad (13)$$

$$\left(\frac{b\omega}{U_0}\right) \upsilon^*_{t^*} + u^* \upsilon^*_\zeta + \left(\frac{b\omega\Delta}{U_0}\right)(\upsilon^* - \dot{H}\eta)\frac{\upsilon^*_\eta}{H} = -\left(\frac{U_0}{a_0\omega\Delta}\right)\frac{\phi^*_\eta}{H} + \left(\frac{\nu b}{U_0 a_0^2}\right)\left(\upsilon^*_{\zeta\zeta}\delta^2 + \frac{\upsilon^*_{\eta\eta}}{H^2}\right) \quad (14)$$

$$\left(\frac{U_0}{b\omega\Delta}\right) u^*_\zeta + \frac{\upsilon^*_\eta}{H} = 0 \quad (15)$$

$$\begin{aligned} &\text{at} \quad \eta = 1 \quad \text{and} \quad \eta = 0 \quad u^* = 0, \\ &\text{at} \quad \eta = 1 \quad \upsilon^* = \dot{H}, \\ &\text{at} \quad \eta = 0 \quad \upsilon^* = 0. \end{aligned} \quad (16)$$

The non-dimensional number $\frac{\nu b}{U_0 a_0^2}$ appearing in the last terms of the right-hand-side can be rewritten as $\frac{1}{\mathrm{Re}\,\delta}$ with $\mathrm{Re} = \frac{U_0 a_0}{\nu}$.

Let us now consider the possibility of finding a self-similar solution to this problem as expressed by equation (6). In that case, we have:

$$u^*(\zeta, \eta, t^*) = u^*_0(\eta, t^*) + u^*_1(\eta, t^*)\zeta \quad (17)$$

Considering the condition established by equation (10) and boundary conditions, it is found that:

$$\phi^*(\zeta, \eta, t^*) = \phi^*_0(\eta, t^*) + \phi^*_1(t^*)\zeta + \phi^*_2(t^*)\zeta^2 \quad (18)$$

Now, the non-dimensional equations for the self-similar solutions for $\delta \ll 1$ can be written as:

$$\left(\frac{b\omega}{U_0}\right) u^*_{0t^*} + u^*_0 u^*_1 + \left(\frac{b\omega}{U_0}\right)\Delta(\upsilon^* - \dot{H}\eta)\frac{u^*_{0\eta}}{H} = -\phi^*_1 + \left(\frac{1}{\mathrm{Re}\,\delta}\right)\frac{u^*_{0\eta\eta}}{H^2} \quad (19)$$

$$\left(\frac{b\omega}{U_0}\right) u^*_{1t^*} + u^{*2}_1 + \left(\frac{b\omega}{U_0}\right)\Delta(\upsilon^* - \dot{H}\eta)\frac{u^*_{1\eta}}{H} = -2\phi^*_2 + \left(\frac{1}{\mathrm{Re}\,\delta}\right)\frac{u^*_{1\eta\eta}}{H^2} \quad (20)$$

$$\left(\frac{b\omega}{U_0}\right) \upsilon^*_{t^*} + \left(\frac{b\omega}{U_0}\right)\Delta(\upsilon^* - \dot{H}\eta)\frac{\upsilon^*_\eta}{H} = -\left(\frac{U_0}{a_0\omega\Delta}\right)\frac{\phi^*_{0\eta}}{H} + \left(\frac{1}{\mathrm{Re}\,\delta}\right)\frac{\upsilon^*_{\eta\eta}}{H^2} \quad (21)$$

$$\left(\frac{U_0}{b\omega\Delta}\right) u^*_1 + \frac{\upsilon^*_\eta}{H} = 0 \quad (22)$$

with boundary conditions:

$$\begin{aligned} &\text{at} \quad \eta = \pm 1 \quad u^*_0 = u^*_1 = 0, \\ &\text{at} \quad \eta = 1 \quad \upsilon^* = \dot{H}, \\ &\text{at} \quad \eta = 0 \quad \upsilon^* = 0 \end{aligned} \quad (23)$$

The value of u^*_0 is associated with a flow that depends on the imposed external gradient pressure ϕ^*_1. An interesting aspect of this set of equations is that the solution for u^*_2, ϕ^*_2 and υ are independent of u^*_0, as the solutions of equations (20)–(22) are decoupled from (19).

3.2.2. The inviscid solution

The inviscid flow assumption is obtained when assuming $\frac{1}{\mathrm{Re}\,\delta} \approx 0$ and relaxing the first condition of equation (23). The solution of the problem is assumed to be self-similar and to satisfy condition 3. In our case, this determines that:

$$\upsilon_{(\eta,t)} = \dot{a}\eta \quad (24)$$

$$u_{(x,t)} = U_{(t)} - \frac{\dot{a}}{a}x \quad (25)$$

$$\Phi_{(x,\eta,t)} = \Phi_{0(\eta,t)} + \Phi_{1(t)}x + \Phi_{2(t)}x^2 \quad (26)$$

where:

$$\Phi_{0(\eta,t)} = \phi_{c(t)} - \frac{\ddot{a}a}{2}\eta^2 \quad (27)$$

$$\Phi_{1(t)} = U_{(t)}\frac{\dot{a}}{a} - \dot{U}_{(t)} \quad (28)$$

$$\Phi_{2(t)} = \frac{1}{2}\left[\frac{\ddot{a}}{a} - 2\left(\frac{\dot{a}}{a}\right)^2\right] \quad (29)$$

Notice that the pressure adopts a quadratic dependence on the x-coordinate and that the pressure changes with the transverse coordinate for a fixed value of x. $U(t)$ represents the value of the velocity at the middle length of the channel and $\phi_c(t)$ is the

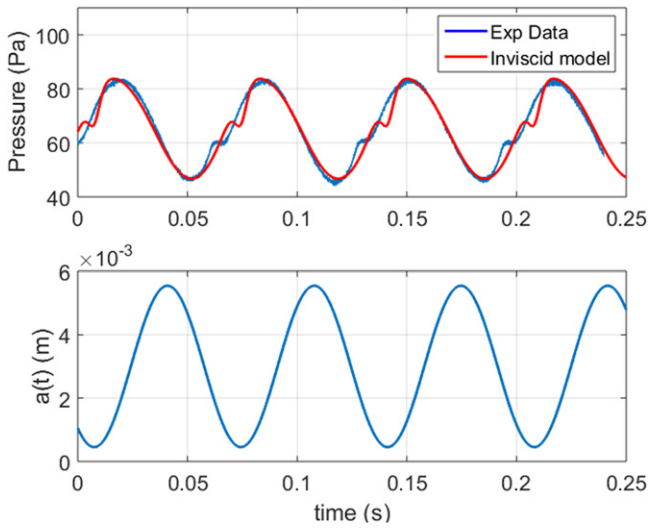

Figure 5. Pressure at the midlength on surface of the lower mass. Experiments vs fitted inviscid model. Parameters in equation (31): $m = 0.124$ kg; $k = 1082$ N m^{-1}; $\gamma_M = 0.1317$ Ns m^{-1}; $y_0 = 0.0039m$.

pressure at this same streamwise coordinate at the lower mass surface. Functions $U(t)$ and $\phi_c(t)$ are related functions that depend on conditions at the channel ends, but not on x.

Considering the equation of kinetic power conservation in its integral form one can easily deduce:

$$\Phi_{c(t)} = \frac{3}{4}{U_{(t)}}^2 + \frac{7}{48}L^2\left(\frac{\dot{a}}{a}\right)^2 + \frac{1}{12}\dot{a}^2 - \frac{L^2}{24}\frac{\ddot{a}}{a} + \frac{1}{2}a\ddot{a} \tag{30}$$

Hence, this expression links the functions $U(t)$ and $\phi_c(t)$ in the assumption of inviscid flow.

4. Discussion

This section proposes the analysis of experimental data based on results issued from the inviscid solution, since the value of $\mathrm{Re}\,\delta \sim 10^2$. The objective is to bring some light on the role played by the non-steady terms appearing in conservation equations in the dynamics. However, this approach has important limitations.

Different studies with a fully developed fow (Espìn and Papageorgiou [51], Hall and Papageorgiou [50]) showed that the pressure-driven flow U_0 is symmetric around $\eta = 0$, as well as periodic with the same period as $a(t)$ for small values of Re. As Re increases the amplitude of the oscillations is also found to increase. This behavior remains unaltered until a critical value $\mathrm{Re_S}$ is reached, above which the solution is no longer symmetric. Espin and Papageorgiou [51] quantified the location of the change of stability of horizontal velocity through a symmetry-breaking bifurcation index $I(\mathrm{Re}, \Delta)$. They showed that at $\mathrm{Re_S} \approx 20$ there is a pitchfork bifurcation to a solution with $I(0.2 < \Delta < 0.4) \neq 0$. At the same time, when these instabilities start to prevail, the flow is no longer 2D.

Instability analysis for cases when boundary layers remain very thin compared to the gap height along the cycle has not yet been reported. Thus, it is not immediate to conclude that similar instabilities as those mentioned above could then develop.

For this reason, and instead of proposing a model providing a full description of the physics involved, we focus our discussion on whether the inviscid solution leaves a significant footprint on the dynamics of the fluid-structure interaction in the experiments.

In our experiments, the movement of the mass was accompanied by a slight rotation in the xy plane. The linear term with $\Phi_1(t)$ contributes to explaining this effect. Also, note that the quadratic term $\Phi_2(t)$ prevails when $a(t)$ attains a minimum value, indicating that the forcing and rotating trend of the mass diminishes as the gap narrows. This is what we observe in figure 3.

We focus on the movement in the vertical direction, and propose that the dynamics of the mass be governed by a law of the type:

$$m\ddot{y}_M + 2\gamma_M\dot{y}_M - k(y_M - y_0) = -mg + F_{aer}(t) \tag{31}$$

with:

$$F_{aer}(t) = -\rho D\int_{-L/2}^{L/2}\phi_{(t,\eta=1)}\mathrm{d}x \tag{32}$$

with D the size of the mass in the z-direction. Note that we disregard here the effect of the lateral walls of the channel.

Considering the equations of the inviscid case, the value of this force equals

$$F_{aer}(t) = \rho LD\left[\frac{3}{4}{U_{(t)}}^2 + \frac{L^2}{16}\left(\frac{\dot{a}}{a}\right)^2 + \frac{\dot{a}^2}{12}\right] \tag{33}$$

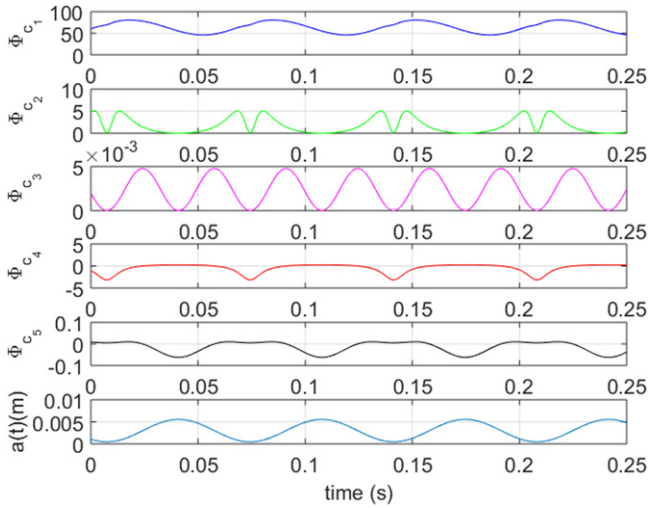

Figure 6. Pressure at the midlength on the surface of the lower mass. Contribution of the different terms Φ_{c_i} of the equation inviscid model in Pa. The subindex i indicates the position of the term in the left-hand side of the equation (30). Parameters in equation (31): $m = 0.124$ kg; $k = 1082$ N m^{-1}; $\gamma_M = 0.1317$ Ns m^{-1}; $y_0 = 0.0039m$.

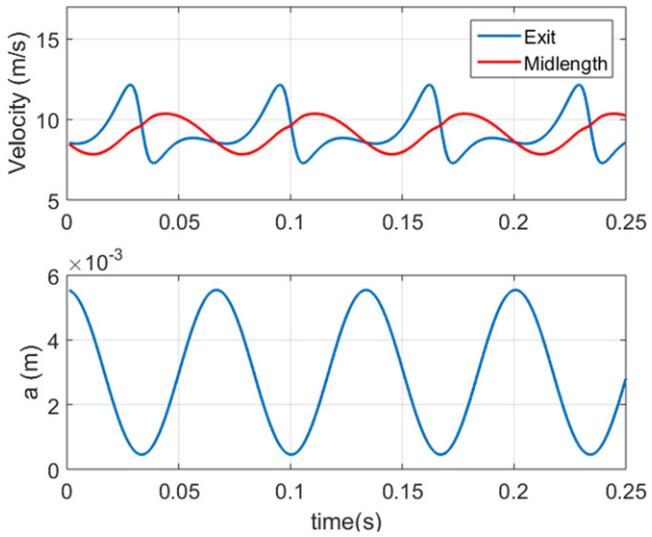

Figure 7. Results of the inviscid model for the flow velocity at the exit ($x = b$) and at the midlength ($x = 0$). Parameters in equation (31): $m = 0.124$ kg; $k = 1082$ N m^{-1}; $\gamma_M = 0.1317$ Ns m^{-1}; $y_0 = 0.0039m$.

Let us now simplify the experimental law of motion of the masses with an expression of the type:

$$a(t) = a_0(1 + \Delta \sin(\omega t)). \tag{34}$$

This law agrees quite well with the recorded mass motion of our experiments when $a_0 = 0.003m$, $\Delta = 0.85$, and $\omega = 93.9$ s^{-1}.

Substituting this expression in equations (30)–(32) and with the data of elastic constant, mass, and damping coefficient of our system we can find the values of $\Phi_c(t)$ and of the flow rate at the exit of the channel. For the pressure, figure 5 compares the recorded experimental values of Φ_c and the one using the inviscid approach.

These curves are obtained with the following parameters in equation (31): $m = 0.124$ kg; $k = 1082$ N m^{-1}; $\gamma_M = 0.1317$ Ns m^{-1}; $y_0 = 0.0039m$. The agreement of model and experimental results observed in figure 5 is surprisingly good. The satisfactory agreement is partly due to a damping coefficient that is only $\sim$10% of the recorded value. This is not anomalous, since viscous effects are being neglected. An increase in the aerodynamic forcing should increase the viscous effects, leading to larger values of this coefficient.

Figure 6 shows the contributions of each term in equation (30). The first and second terms are dominant. To better understand these two terms, figure 7 represents the velocity at the midlength ($x = 0$) and the velocity at the exit of the channel ($x = b$). The difference between both functions indicates the influence of the squeeze flow produced by the moving

plates and the relative weight of this flow compared to the flow produced by the externally imposed pressure gradient. The second term explains the origin of the wiggle observed on the pressure signal in figure 5. In the slight phase delay of the wiggle, different factors can come into play, e.g. the incidence of the boundary layer when the channel height becomes quite narrow.

5. Conclusions

This paper presented an experimental and analytical study of a parallel-sided channel with one wall pulsating periodically. We observed that the oscillations induced by the flow of the mass that limits one side of the channel occurred at a frequency close to the natural frequency of the system. The gap varied following an almost sinusoidal wall of motion. The mean velocity in the channel attained a relatively high value compared to the horizontal squeeze flow produced by the oscillating mass.

The analytical study we propose was based on the assumption of a self-similar behavior of the flow inside the channel. The study allowed us to analyze the nature of the flow-induced oscillation in the context of an inviscid flow assumption.

This theoretical framework enabled gaining physical insight into some aspects of the flow-induced movement. The rotating trend of the mass was explained in terms of the quadratic dependence of the pressure with streamwise coordinate. A very good agreement was obtained between the theory and the experimental pressure, measured at the midlength of the channel. This was achieved when the damping coefficient was assigned a value that was substantially lower than the recorded one, indicating that the viscous effects should not be seen as the only factor producing a significant forcing of the mass.

Our article has privileged a study based on analytical solutions. Even if interesting, numerical approaches are delicate and have issues associated with the accuracy of the solutions when the oscillation amplitude is large and the gaps are quite narrow. Future work can bring into the analysis some aspects that we have left without consideration and that may have relevance in terms of the physics of the problem, such as the development of three-dimensional effects or the role of downstream flow structures.

Acknowledgments

This research was supported by Conicet, Argentina (postdoctoral scholarship of Dario Alviso). We acknowledge ENSTA-Paris for sharing part of the experimental setup used in this paper.

Conflict of interest

On behalf of all authors, the corresponding author states that there is no conflict of interest.

Data availability statement

All data that support the findings of this study are included within the article (and any supplementary files).

ORCID iDs

Dario Alviso https://orcid.org/0000-0002-6752-4218
Denisse Sciamarella https://orcid.org/0000-0001-5218-3708
Alejandro Gronskis https://orcid.org/0000-0002-7490-4171
Guillermo Artana https://orcid.org/0000-0003-1337-0126

References

[1] Secomb T W 1978 Flow in a channel with pulsating walls *J. Fluid Mech.* **88** 273–88
[2] Arinchin N and Borisevich G Micropumping activity of the extended skeletal muscles (Minsk: Nauka I Technika)
[3] Waters S L 2001 Solute uptake through the walls of a pulsating channel *J. Fluid Mech.* **433** 193–208
[4] Westneat M W, Betz O, Blob R W, Fezzaa K, Cooper W J and Lee W-K 2003 Tracheal respiration in insects visualized with synchrotron x-ray imaging *Science* **299** 558–60
[5] Pedley P H T 1993 Axial dispersion in a channel with oscillating walls *J. Fluid Mech.* **249** 535–55
[6] Elemans C *et al* 2015 Universal mechanisms of sound production and control in birds and mammals *Nat. Commun.* **6** 8978
[7] Grotberg J B and Jensen O E 2004 Biofluid mechanics in flexible tubes *Annu. Rev. Fluid Mech.* **36** 121–47
[8] Stephanoff K D, Pedley T J, Lawrence C J and Secomb T W 1983 Fluid flow along a channel with an asymmetric oscillating constriction *Nature* **305** 692–5
[9] Pedley T J and Stephanoff K D 1985 Flow along a channel with a time-dependent indentation in one wall: the generation of vorticity waves *J. Fluid Mech.* **160** 337–67
[10] Ralph M E and Pedley T J 1988 Flow in a channel with a moving indentation *J. Fluid Mech.* **190** 87–112
[11] Ralph M E and Pedley T J 1989 Viscous and inviscid flows in a channel with a moving indentation *J. Fluid Mech.* **209** 543–66
[12] Demirdžić I and Perić M 1990 Finite volume method for prediction of fluid flow in arbitrarily shaped domains with moving boundaries *Int. J. Numer. Methods Fluids* **10** 771–90
[13] Ben-Mansour R, Habib M A and Qaiyum Shaik A 2009 Modeling of fluid flow in a tube with a moving indentation *Comput. Fluids* **38** 818–29
[14] Smith S L and Thomson S L 2013 Influence of subglottic stenosis on the flow-induced vibration of a computational vocal fold model *J. Fluid Struct.* **38** 77–91
[15] Howe M S and McGowan R S 2009 Analysis of flow-structure coupling in a mechanical model of the vocal folds and the subglottal system *J. Fluid Struct.* **25** 1299–317
[16] Horáček J, Šidlof P and Švec J 2005 Numerical simulation of self-oscillations of human vocal folds with Hertz model of impact forces *J. Fluid Struct.* **20** 853–69
[17] Chen Y, Li Z, Chang S, Rousseau B and Luo H 2020 A reduced-order flow model for vocal fold vibration: from idealized to subject-specific models *J. Fluid Struct.* **94** 102940

[18] Bhattacharya P and Siegmund T 2014 Validation of a flow-structure-interaction computation model of phonation *J. Fluid Struct.* **48** 169–87
[19] Sciamarella D, Chisari E, Artana G, Bailly L and Pelorson X 2008 Separated flow behavior in an *in vitro* rigid model of the laryngeal channel *J. Acoust. Soc. Am.* **123** 3577
[20] Krebs F, Silva F, Sciamarella D and Artana G 2012 A three-dimensional study of the glottal jet *Exp. Fluids* **52** 1133–47
[21] Fletcher N H 1993 Autonomous vibration of simple pressure-controlled valves in gas flows *J. Acoust. Soc. Am.* **93** 2172–80
[22] Sciamarella D and Artana G 2009 A water hammer analysis of pressure and flow in the voice production system *Speech Commun.* **51** 344–51
[23] Krane M H, Barry M and Wei T 2010 Dynamics of temporal variations in phonatory flow *J. Acoust. Soc. Am.* **128** 372–83
[24] Bagheri Sarvestani A, Goshtasbi Rad E and Iravani K 2018 Numerical analysis and comparison of flow fields in normal larynx and larynx with unilateral vocal fold paralysis *Comput. Methods Biomech. Biomed. Eng.* **21** 532–40
[25] Hamza E A and MacDonald D A 1981 A fluid film squeezed between two parallel plane surfaces *J. Fluid Mech.* **109** 147–60
[26] Blyth M G 2007 Effect of pulsations on two-layer channel flow *J. Eng. Math.* **59** 123–37
[27] Moss E A, Krassnokutski A, Skews B W and Paton R T 2011 Highly transient squeeze-film flows *J. Fluid Mech.* **671** 384
[28] Mittra T K and Prasad S N 1973 On the influence of wall properties and Poiseuille flow in peristalsis *J. Biomech.* **6** 681–93
[29] Pozrikidis C 1987 A study of peristaltic flow *J. Fluid Mech.* **180** 515–27
[30] Aboelkassem Y and Staples A E 2013 A bioinspired pumping model for flow in a microtube with rhythmic wall contractions *J. Fluid Struct.* **42** 187–204
[31] D'Netto W and Weaver D 1987 Divergence and limit cycle oscillations in valves operating at small openings *J. Fluid Struct.* **1** 3–18
[32] El Bouzidi S, Hassan M and Ziada S 2018 Experimental characterisation of the self-excited vibrations of spring-loaded valves *J. Fluid Struct.* **76** 558–72
[33] Habing R A and Peters M C A M 2006 An experimental method for validating compressor valve vibration theory *J. Fluid Struct.* **22** 683–97
[34] El Bouzidi S, Hassan M and Ziada S 2019 Acoustic methods to suppress self-excited oscillations in spring-loaded valves *J. Fluid Struct.* **85** 126–37
[35] Shi Y, Yang S, Pan X and Liu Y 2019 Investigation on dynamic characteristics of a plate-type discharge valve in a diaphragm pump for SCR system by two-way FSI model *Proc. Inst. Mech. Eng.* D **234** 0954407019862168
[36] Vainshtein P and Shapiro M 2008 Aerodynamic focusing in a channel with oscillating walls *J. Aerosol Sci.* **39** 929–39
[37] Drazin P G and Riley N 2006 *The Navier–Stokes Equations: A Classification of Flows and Exact Solutions* vol 334 (Cambridge: Cambridge University Press)
[38] Rott N 1956 Unsteady viscous flow in the vicinity of a stagnation point *Q. Appl. Math.* **13** 444–51
[39] Blyth M G and Hall P 2003 Oscillatory flow near a stagnation point *SIAM J. Appl. Math.* **63** 1604–14
[40] Kuzma D C 1968 Fluid inertia effects in squeeze films *Appl. Sci. Res.* **18** 15–20
[41] Ishizawa S 1966 The axi-symmetric laminar flow in an arbitrarily shaped narrow gap: (2nd report, theoretical analysis for the downstream region) *Bull. JSME* **9** 86–103
[42] Tichy J A 1981 An approximate analysis of fluid inertia effects in axisymmetric laminar squeeze film flow at arbitrary Reynolds number *Appl. Sci. Res.* **37** 301–12
[43] Stuart J T, DiPrima R, Eagles P and Davey A 1990 On the instability of the flow in a squeeze lubrication film *Proc. R. Soc.* A **430** 347–75
[44] Aristov S N and Knyazev D V 2012 Viscous fluid flow between moving parallel plates *Fluid Dyn.* **47** 476–82
[45] Singh P, Radhakrishnan V and Narayan K A 1990 Squeezing flow between parallel plates *Ing.-Arch.* **60** 274–81
[46] Petrov A G 2012 Exact solution of the Navier–Stokes equations in a fluid layer between the moving parallel plates *J. Appl. Mech. Tech. Phys.* **53** 642–6
[47] Šidlof P, Doaré O, Cadot O and Chaigne A 2011 Measurement of flow separation in a human vocal folds model *Exp. Fluids* **51** 123–36
[48] Konarasinghe W and Konarasinghe K 2021 Model development for damped and forced type of oscillations in time series *J. New Front. Appl. Math. Stat.* **2** 20–35
[49] Hall P 1978 The linear stability of flat Stokes layers *Proc. R. Soc.* A **359** 151–66
[50] Hall P and Papageorgiou D T 1999 The onset of chaos in a class of Navier–Stokes solutions *J. Fluid Mech.* **393** 59–87
[51] Espìn L and Papageorgiou D T 2012 Viscous pressure-driven flows and their stability in channels with vertically oscillating walls *Phys. Fluids* **24** 023604